SOILS AND FOUNDATIONS Vol. 21, No. 1, Mar. 1981
Japanese Society of Soil Mechanics and Foundation Engineering

MULTI-DIMENSIONAL ELASTO-PLASTIC CONSOLIDATION ANALYSIS BY FINITE ELEMENT METHOD

TAMOTSU MATSUI* and NOBUHARU ABE**

ABSTRACT

An analytical method due to the hybrid finite element formulation is presented for the multi-dimensional elasto-plastic consolidation analysis. To facilitate a reliable consolidation analysis of K_0-consolidated clay layer, an elasto-plastic analytical model is also proposed, which has a yield function with no singularity satisfying the K_0-strain condition on the K_0-line, followed by showing its reasonableness and advantage in numerical computations.

To deal with a more realistic consolidation analysis, the presented method is also characterized by the ability to analyze such cases that the drainage is permitted during incremental loading and that the permeability suddenly changes in the layer.

Multi-dimensional elasto-plastic consolidation analysis is carried out for partially loaded ground models. The resulting deformation and stress path behaviors substantiate the validity of the presented analytical technique, which brings out some behaviors reflecting the real mechanism of consolidation of clay.

Key words: consolidation, deformation, dilatancy, effective stress, finite element method, plasticity, pore pressure, soft ground, stress path

IGC: E 1/E 2

INTRODUCTION

In foundation engineering the one-dimensional consolidation theory of Terzaghi is most commonly employed to estimate the progress of consolidation and settlement of clayey ground. This theory is based, however, on assumptions that the soil has a linear elastic deformability and that both its displacement and the flow of water through the porous medium occur only in the vertical direction. The construction of an embankment on a soft clay layer rarely causes such one-dimensional behaviors in the layer, but generally nonlinear consolidation behaviors involving lateral displacement. Thus, to properly estimate those phenomena, it may be indispensable to introduce a multi-dimensional consolidation analysis considering a nonlinear stress-strain relation.

It is well-known that the Terzaghi-Rendulic theory of multi-dimensional consolidation inadequately represents the continuity of soil mass. On the other hand, the Biot theory (Biot, 1941) is preferable from this point of view, because it couples total stress equilib-

* Associate Professor, Department of Civil Engineering, Osaka University, Yamada-kami, Suita, Osaka 565.
** Research Associate, ditto.
Written discussions on this paper should be submitted before January 1, 1982.

rium to strain-compatibility during consolidation. It cannot be avoided, however, that the resulting equations are complicated. Although several closed form solutions to Biot's equations have been published over the year, such solutions are limited to problems with simple geometry and material properties. Then, a numerical method must be applied to solve more complicated ones.

Development of the finite element method provided the necessary tool for treatment of general consolidation problems with no restrictions on geometory, material properties and boundary condition. Finite element formulations of the Biot theory of consolidation facilitate its application and have made it possible to introduce into the design process on evaluation of the time rate of settlement for a variety of two and three dimensional problems.

The first finite element formulation of the Biot theory was that of Sandhu and Wilson (1969), which was based on the Gurtin's convolution variational theorem. Since then, Yokoo et al. (1971 a, b), Hwang et al. (1971) and Valliappan and Lee (1975) analyzed the process of consolidation by similar techniques, and Ghaboussi and Wilson (1973) extended the functional formulation to include compressible pore fluid. Hwang et al. (1972) carried out a formulation due to Galerkin's method, and obtained the same result as Sandhu and Wilson.

On the other hand, Christian and Boehmer (1970) succeeded in another approach of the finite element formulation of consolidation, applying a generalized variational principle to the static equations of equilibrium in terms of unknown displacements and pore pressures. The time-dependent change in both stresses and pore pressures during consolidation is then introduced by applying the continuity equation in a finite difference form. Such a technique has been proposed by Herrmann (1965) and used by Christian (1968) in the solution of static stress distribution for undrained, incompressible soils.

The major shortcoming of all the formulations described above is, however, that they do not account for the nonlinearity of the stress-strain behavior of the soil. Although more realistic elasto-plastic models in the constitutive relation of the soil are recently developed, there are little attempts on the application of these models to the consolidation analysis, except by Akai and Tamura (1977). The elasto-plastic model applied by them, however, does not satisfy requisitions of deformation characteristics, which must be involved in an elasto-plastic model for the consolidation analysis of K_0-consolidated layer. Thus, their results may not be reliable enough for more detailed discussion.

In this paper, the authers give a sophisticated technique of multi-dimensional elasto-plastic consolidation analysis due to the finite element method. A reasonable analytical model of soft clay is proposed, which is applicable to the consolidation analysis of the normally K_0-consolidated clay layer. Then, the availability of the proposed analytical method of consolidation is demonstrated by showing such analytical results for a partially loaded ground model as time-dependent behaviors, especially stress path behaviors during consolidation.

FINITE ELEMENT FORMULATION

Biot's fundamental equations of consolidation under plane strain condition are represented in the following. That is, the equations of equilibrium condition are given as follows:

$$\left.\begin{aligned}\frac{\partial \sigma_x'}{\partial x}+\frac{\partial \tau_{xy}}{\partial y}+\frac{\partial u}{\partial x}=0\\ \frac{\partial \sigma_y'}{\partial y}+\frac{\partial \tau_{xy}}{\partial x}+\frac{\partial u}{\partial y}=0\end{aligned}\right\} \quad (1)$$

in which σ_x', σ_y' and τ_{xy} are the effective normal stresses in the directions of x and y and the shear stress induced by a surcharge, respectively, and u is the excess pore water pressure. Applying Darcy's law, the equation of continuity condition is given as follows:

$$\frac{\partial v}{\partial t}+\frac{1}{\gamma_w}\left(k_x\frac{\partial^2 u}{\partial x^2}+k_y\frac{\partial^2 u}{\partial y^2}\right)=0 \tag{2}$$

in which v is the volumetric strain, t is the real time, k_x and k_y are the coefficients of permeability in the directions of x and y, respectively, and γ_w is the unit weight of pore water. Thus, Eqs. (1) and (2) compose the fundamental equations of consolidation. Discretization of the equation of equilibrium condition according to the principle of virtual work gives the following incremental relation.

$$\Delta \boldsymbol{F}=\boldsymbol{K}\Delta \boldsymbol{U}+\boldsymbol{L}\Delta u \tag{3}$$

in which $\Delta \boldsymbol{F}$ and $\Delta \boldsymbol{U}$ are the incremental vectors of the equivalent nodal force and the nodal displacement, respectively, $\boldsymbol{K}$ is the stiffness matrix of element, $\boldsymbol{L}$ is the vector transforming the nodal displacement increment into the volume change of element ΔV, and Δu is the excess pore water pressure increment. According to the definition, the volume change of element is given as follows:

$$\Delta V=\boldsymbol{L}^T\Delta \boldsymbol{U} \tag{4}$$

Substituting the evaluated volume change of element by Eq. (2) into Eq. (4), Eqs. (3) and (4) make simultaneous equations of both unknown of $\Delta \boldsymbol{U}$ and Δu. The solution of consolidation can be obtained by evaluating ΔV and solving the simultaneous equations step by step as the consolidation progresses. To solve Eq. (2) due to the calculus of finite difference, the distribution of the representative excess pore water pressure $\bar{u}$, which is defined by Eq. (5), is spacially given by the following Eq. (6), according to Christian and Boehmer (1970).

$$\bar{u}=\{(1-\theta)u_t+\theta u_{t+\Delta t}\} \tag{5}$$

$$\bar{u}=\alpha_1+\alpha_2 x+\alpha_3 y+\alpha_4 x^2+\alpha_5 y^2 \tag{6}$$

in which u_t and $u_{t+\Delta t}$ are the excess pore water pressures at the times $t=t$ and $t=t+\Delta t$, respectively, θ $(0\leqq\theta\leqq 1)$ is a constant on the difference approximation, and α_1, α_2, α_3, α_4 and α_5 are the indeterminate coefficients, which are determined in a quadrilateral element i and the four surrounding elements designated by j, k, l and m, respectively, as shown in Fig. 1. By designating the representative excess pore water pressures of the five elements by $\bar{u}_i, \bar{u}_j, \bar{u}_k, \bar{u}_l$ and $\bar{u}_m$, and the locations of centers of the four surrounding elements from the center of element i by $(\bar{x}_j, \bar{y}_j)$, $(\bar{x}_k, \bar{y}_k)$, $(\bar{x}_l, \bar{y}_l)$ and $(\bar{x}_m, \bar{y}_m)$, as shown in Fig. 1, the vector $\bar{\boldsymbol{u}}$ of representative pore water pressure is represented as follows:

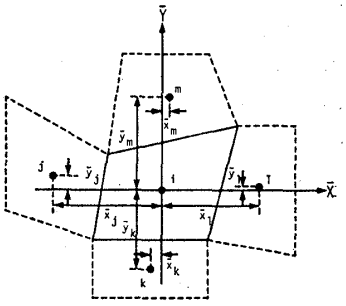

Fig. 1. Local co-ordinate used in evaluating rate of flow

$$\bar{\boldsymbol{u}}=\begin{Bmatrix}\bar{u}_i\\ \bar{u}_j\\ \bar{u}_k\\ \bar{u}_l\\ \bar{u}_m\end{Bmatrix}=\begin{pmatrix}1 & 0 & 0 & 0 & 0\\ 1 & \bar{x}_j & \bar{y}_j & \bar{x}_j^2 & \bar{y}_j^2\\ 1 & \bar{x}_k & \bar{y}_k & \bar{x}_k^2 & \bar{y}_k^2\\ 1 & \bar{x}_l & \bar{y}_l & \bar{x}_l^2 & \bar{y}_l^2\\ 1 & \bar{x}_m & \bar{y}_m & \bar{x}_m^2 & \bar{y}_m^2\end{pmatrix}\begin{Bmatrix}\alpha_1\\ \alpha_2\\ \alpha_3\\ \alpha_4\\ \alpha_5\end{Bmatrix}=\boldsymbol{B}\boldsymbol{\alpha} \tag{7}$$

Then,

$$\boldsymbol{\alpha}=\boldsymbol{B}^{-1}\bar{\boldsymbol{u}} \tag{8}$$

Substitution of Eq. (16) into Eq. (2), and then its transformation in consideration of Eq. (8) give the fo'lowing equation.

$$\begin{aligned}\Delta V&=-\frac{\Delta t V}{\gamma_w}(2k_x\alpha_4+2k_y\alpha_5)\\&=-\frac{2\Delta t V}{\gamma_w}(k_x\boldsymbol{b}_4^T\bar{\boldsymbol{u}}+k_y\boldsymbol{b}_5^T\bar{\boldsymbol{u}})\\&=-\boldsymbol{C}^T\bar{\boldsymbol{u}}\end{aligned} \tag{9}$$

in which $\boldsymbol{C}=(2\,\Delta tV/\gamma_w)(k_x\boldsymbol{b}_4+k_y\boldsymbol{b}_5)$, Δt is the small increment of time, V is the volume of element, and $\boldsymbol{b}_4$ and $\boldsymbol{b}_5$ are the vectors of the fourth and fifth rows of $\boldsymbol{B}^{-1}$, respectively. Transformation of Eq. (3) using the relation of $\Delta u=u_{t+\Delta t}-u_t$, and also substitution of Eq. (9) into Eq. (4), referring the definition of $\bar{u}$ in Eq. (5), give the following equations.

$$\left.\begin{aligned}&\Delta\boldsymbol{F}+\boldsymbol{L}u_{i,t}=\boldsymbol{K}\Delta\boldsymbol{U}+\boldsymbol{L}u_{i,t+\Delta t}\\&-(1-\theta)\boldsymbol{C}^T\boldsymbol{u}_t=\boldsymbol{L}^T\Delta\boldsymbol{U}+\theta\boldsymbol{C}^T\boldsymbol{u}_{t+\Delta t}\end{aligned}\right\} \tag{10}$$

in which $\boldsymbol{u}_t$ and $\boldsymbol{u}_{t+\Delta t}$ are the vectors of excess pore water pressure at the times $t=t$ and $t=t+\Delta t$, respectively. Both of equations in Eq. (10) represent the incremental relat'ons of equilibrium and continuity condition, respectively, which should be satisfied in the element i. Assemblage of such incremental relations of all elements as in Eq. (10) gives their overall extended stiffness matrix. In Eq. (10), $\theta=0$, and $\theta=1$ correspond to the forward and backward differences, respectively. In the former ($\theta=0$), the excess pore water pressure increment Δu is represented by an explicit form, and then Eq. (10) is simplified as follows:

$$\left.\begin{aligned}&\Delta\boldsymbol{F}=\boldsymbol{K}\Delta\boldsymbol{U}+\boldsymbol{L}\Delta u\\&-\boldsymbol{C}^T\boldsymbol{u}_t=\boldsymbol{L}^T\Delta\boldsymbol{U}\end{aligned}\right\} \tag{11}$$

When $0<\theta\leqq 1$, Δu can not be represented by an explicit form, and then Eq. (10) left in the implicit form must be used in the analysis. In this paper, the midpoint difference ($\theta=1/2$) is used, which may be most preferable from the viewpoint of both the accuracy and the stability of solution.

The presented formulation herein demands the use of quadrilateral elements. In the following numerical analysis, the quadrilateral element composed of four triangular elements is used, which is proposed by Wilson (1965). A central nodal point in a quadrilateral element is eliminated by the static condensation. Thus, the stress and pore water pressure are always constant within a quadrilateral element.

The consolidation analysis is carried out by solving Eq. (10) in each small time increment. In case where the stress-strain relation of material is nonlinear, nonlinear behavior is approximated as piecewise linear in each time increment, and then the optimum time increment should be carefully selected so as to make this approximation valid. Consequently, the incremental procedure is used as the technique of nonlinear analysis.

ANALYTICAL MODEL FOR SOFT CLAY

General Remarks

There are some existing elasto-plastic models of clay which can be applied to the numerical analysis. They are Cam-clay model proposed by Roscoe et al. (1963), an extended model to the anisotropic consolidated state, named as anisotropic Cam-clay model in this paper and a model by Ohta and Hata (1971), which is equivalent to both models described above.

It can not be recommended that these models are applied to the consolidation analysis of the K_0-consolidated clay layer, because of the following reasons. That is, the plastic strain increment ratio in Cam-clay model do not satisfy the K_0-strain condition during K_0-consolidation. Thus, the K_0-consolidation analysis due to Cam-clay model gives a contrary result to the fact that the effective stress path moves on the K_0-line during K_0-consolidation. Because both active and passive states bounded on the K_0-line are mixed during the consolidation deformation in a K_0-consolidated clay layer, Cam-clay model, in which both states are bounded at the isotropic state, may not be adequately applied to such a kind of consolidation analysis. On the other hand, in both models of anisotropic Cam-clay and Ohta-Hata the active and passive states are bounded on the K_0-line. Their yield function has, however, a singular point at $\eta=\eta_{k0}$, i.e. their yield curve forms a cusp on the K_0-line. This means that their plastic strain increment ratio and hardening coefficient can not be uniquely defined on the K_0-line, and they change suddenly and discontinuously on both sides of it. Then, the application of these models to the K_0-consolidation analysis yields sawteethly oscillating stress paths, depending on the time increment used in the analysis. In the deformation analysis of K_0-consolidated clay layer up to the final stage of consolidation, it is necessary to take larger time increments with progressing consolidation, because of the limitation of the computing time in a computer. Thus, the resulting effective stress path oscillates more strongly, and it may be hopeless to obtain a smooth stress path, which is a requisition for the accurate result.

As described above, those models developed by the shear test result of soil have some troubles for the consolidation analysis around the initial K_0-state. It is needless to say that the analytical ability of a model around the initial K_0-state is very important in the K_0-consolidation analysis. In this chapter a reasonable analytical model will be presented, which has no troubles as described above and is applicable to the deformation analysis of the K_0-consolidated clay layer.

Presentation of Analytical Model

Yield locus and state boundary surface: First, parameters of the stress and the strain are defined. Designating the mean effective principal stress and the generalized shear stress by p' and q, respectively,

$$p'=\frac{\sigma_1'+\sigma_2'+\sigma_3'}{3} \tag{12}$$

$$q=\frac{1}{\sqrt{2}}\{(\sigma_1'-\sigma_2')^2+(\sigma_2'-\sigma_3')^2+(\sigma_3'-\sigma_1')^2\}^{1/2} \tag{13}$$

in which σ_1', σ_2' and σ_3' are the effective principal stresses. Designating the volumetric strain and the generalized shear strain by v and γ, respectively,

$$v=\varepsilon_1+\varepsilon_2+\varepsilon_3 \tag{14}$$

$$\gamma=\frac{\sqrt{2}}{3}\{(\varepsilon_1-\varepsilon_2)^2+(\varepsilon_2-\varepsilon_3)^2+(\varepsilon_3-\varepsilon_1)^2\}^{1/2} \tag{15}$$

in which ε_1, ε_2 and ε_3 are the principal strains.

Next, an analytical model based on the associated flow rule is derived, referring to the concept of Cam-clay model. The plastic strain increment ratio, designated by $1/\psi$, is assumed for the active and passive stress states as follows:

$$\frac{1}{\psi}=\frac{\delta\gamma^p}{\delta v^p}=\frac{\alpha_a}{M_a-\eta} \quad \text{for the active state} \tag{16}$$

$$\frac{1}{\psi}=\frac{\delta\gamma^p}{\delta v^p}=\frac{-\alpha_p}{M_p+\eta} \quad \text{for the passive state} \tag{17}$$

in which the superscript p signifies plastic, α_a and α_p are the parameters for the active and passive states, respectively, η is the stress ratio $(=q/p')$, and M_a and $M_p(>0)$ are the values of η at the critical states in the active and passive states, respectively.

The differential equation of yield function is given as the following equation (Roscoe and Burland, 1968).

$$\frac{\delta p_y'}{p_y'}-\frac{\delta p'}{p'}-\frac{\delta \eta}{\psi+\eta}=0 \tag{18}$$

in which p_y' is the strain hardening parameter. Substitution of Eqs. (16) and (17) into Eq. (18), and then its integration under the initial condition of $p'=p_0'$, $\eta=\eta_{k0}$ and $p_y'=p_{y0}'$, using the condition of normally consolidated state i.e. $p_{y0}'=p_0'$, give the yield functions f_a and f_p for the active and passive states, as follows:

$$f_a=p'\left\{\frac{M_a+(\alpha_a-1)\eta}{M_a+(\alpha_a-1)\eta_{k0}}\right\}^{\alpha_a/(\alpha_a-1)}=p_y' \quad \text{for the active state} \tag{19}$$

$$f_p=p'\left\{\frac{M_p+(1-\alpha_p)\eta_{k0}}{M_p+(1-\alpha_p)\eta}\right\}^{\alpha_p/(1-\alpha_p)}=p_y' \quad \text{for the passive state} \tag{20}$$

in which η_{k0} is η on the K_0-line, and neither of α_a and α_p is unity.

The state boundary surface can be similarly obtained as follows:

$$e_0-e=\lambda \ln\left(\frac{p'}{p_0'}\right)+(\lambda-\kappa)\left(\frac{\alpha_a}{\alpha_a-1}\right)\ln\left\{\frac{M_a+(\alpha_a-1)\eta}{M_a+(\alpha_a-1)\eta_{k0}}\right\}$$

for the active state (21)

$$e_0-e=\lambda \ln\left(\frac{p'}{p_0'}\right)+(\lambda-\kappa)\left(\frac{\alpha_p}{1-\alpha_p}\right)\ln\left\{\frac{M_p+(1-\alpha_p)\eta_{k0}}{M_p+(1-\alpha_p)\eta}\right\}$$

for the passive state (22)

in which e is the void ratio, e_0 is the initial value of e, and λ and κ are the compression and swelling indexes, respectively.

Strain increment ratio and parameters α_a and α_p: The following strain condition must be satisfied in the K_0-consolidation.

$$\frac{\delta \varepsilon_v}{\delta v}=1.0 \tag{23}$$

in which ε_v is the vertical strain. Eq. (23) is a restriction imposed on the total strain. It is assumed, however, to impose a similar restriction each on elastic and plastic strain components, as follows:

$$\frac{\delta \varepsilon_v^e}{\delta v^e}=1.0 \tag{24}$$

$$\frac{\delta \varepsilon_v^p}{\delta v^p}=1.0 \tag{25}$$

in which the superscripts e and p signify elastic and plastic, respectively. Whenever Eqs. (24) and (25) are satisfied, Eq. (23) is valid.

As for the restriction on the elastic strain increment, Eq. (24) is always satisfied if the Poisson's ratio ν of the clay is decided as follows:

$$\nu=\frac{K_0}{1+K_0} \tag{26}$$

in which K_0 is the coefficient of earth pressure at rest. As for the restriction on the plastic strain increment, the following technique is used to satisfy Eq. (25). That is, the plastic strain increment ratio $1/\psi$ must satisfy the following equation at $\eta=\eta_{k0}$.

$$\frac{1}{\psi}=\left(\frac{\delta\gamma^p}{\delta v^p}\right)_{\eta=\eta_{k0}}=\frac{2}{3}\left(\frac{\delta\varepsilon_v^p}{\delta v^p}\right)=\frac{2}{3} \tag{27}$$

The yield function in Eqs. (19) and (20) satisfy Eq. (27) at $\eta=\eta_{k0}$, if the parameters α_a and α_p are decided as follows:

$$\alpha_a=\frac{2}{3}(M_a-\eta_{k0}) \tag{28}$$

$$\alpha_p=-\frac{2}{3}(M_p+\eta_{k0}) \tag{29}$$

Consequently, two yield curves are smoothly connected on the K_0-line and have no singularity there.

On the other hand, introducing the assumption of the energy dissipation used in Cam-clay model, the following equations are valid only at critical state of the presented analytical model.

$$\left.\begin{aligned}\alpha_a&=1.0 \quad \text{at } \eta=M_a\\ \alpha_p&=1.0 \quad \text{at } \eta=-M_p\end{aligned}\right\} \tag{30}$$

The values of parameters α_a and α_p except at both of the initial K_0-state and the critical state are evaluated as a function of stress state, based on shear test results of clays. By this process, such inherent characteristics of clays as the dilatancy and the anisotropy can be introduced into the presented analytical model.

The solid curve in Fig. 2 shows a yield function of the presented analytical model obtained by the technique described above, in which the parameters α_a and α_p are approximated by the hyperbola as a function of the stress ratio η, as shown in Fig. 3. A yield function of the anisotropic Cam-clay model is also shown by the broken curve in Fig. 2, in which $\alpha_a=\alpha_p=1.0$ as shown by the broken line in Fig. 3. It is clear from Fig. 2 that a singular point of the yield function can be found on the K_0-line of anisotropic Cam-clay model, but that no singular point on the yield function of the presented analytical model.

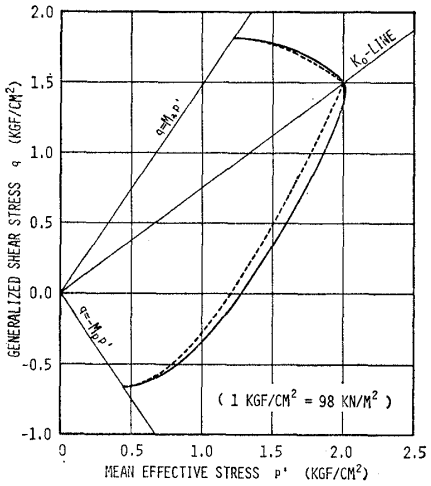

Fig. 2. Yield function of the presented analytical model

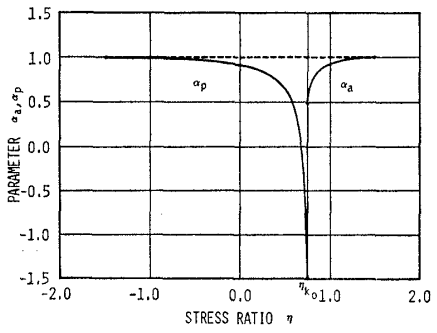

Fig. 3. Approximation of the parameters α_a and α_p by the hyperbola as a function of the stress ratio η

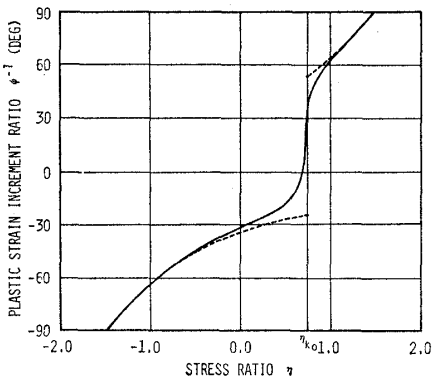

Fig. 4. Variation of the plastic strain increment ratio $1/\psi$ with the stress ratio η

Fig. 4 shows the variation of the plastic strain increment ratio $1/\psi$ with the stress ratio η, in which the solid and broken curves represent those of the presented analytical model and anisotropic Cam-clay model, respectively. It is confirmed from Fig. 4 that the plastic strain increment ratio of the presented analytical model varies continuously and smoothly with the stress ratio, satisfying the K_0-strain condition at $\eta=\eta_{k0}$ i. e. Eq. (27). On the other hand, that of anisotropic Cam-clay model varies suddenly and discontinuously with the stress ratio. Thus, the presented analytical model has not such unreasonableness and difficulty on the numerical analysis of K_0-consolidation as pointed out at the beginning of this chapter.

Stress-strain relation: The associated flow rule and the normality rule are assumed in the presented analytical model. Designating the elastic and elasto-plastic stress-strain matrixes by $\boldsymbol{D}_e$ and $\boldsymbol{D}_{ep}$, respectively, the elasto-plastic stress-strain relation is given as follows:

$$\begin{aligned}\Delta\boldsymbol{\sigma}' &= \boldsymbol{D}_{ep}\Delta\boldsymbol{\varepsilon} \\ &= \left(\boldsymbol{D}_e - \frac{\boldsymbol{D}_e\boldsymbol{a}\boldsymbol{a}^T\boldsymbol{D}_e}{A+\boldsymbol{a}^T\boldsymbol{D}_e\boldsymbol{a}}\right)\Delta\boldsymbol{\varepsilon}\end{aligned} \tag{31}$$

in which

$$\Delta\boldsymbol{\sigma}' = \begin{Bmatrix}\Delta\sigma_x' \\ \Delta\sigma_y' \\ \Delta\tau_{xy}\end{Bmatrix}, \quad \Delta\boldsymbol{\varepsilon} = \begin{Bmatrix}\Delta\varepsilon_x \\ \Delta\varepsilon_y \\ \Delta\gamma_{xy}\end{Bmatrix}, \quad \boldsymbol{a} = \begin{Bmatrix}\dfrac{\partial f}{\partial\sigma_x'} \\ \dfrac{\partial f}{\partial\sigma_y'} \\ \dfrac{\partial f}{\partial\tau_{xy}}\end{Bmatrix},$$

$$\boldsymbol{D}_e = \frac{E(1-\nu)}{(1+\nu)(1-2\nu)}\begin{pmatrix} 1 & \dfrac{\nu}{1-\nu} & 0 \\ \dfrac{\nu}{1-\nu} & 1 & 0 \\ 0 & 0 & \dfrac{1-2\nu}{2(1-\nu)}\end{pmatrix},$$

$$E = \frac{3(1+e)(1-2\nu)p'}{\kappa},$$

$$f = \begin{cases} f_a - p_y' = 0 & \text{for the active state} \\ f_p - p_y' = 0 & \text{for the passive state,}\end{cases}$$

$$A = -\frac{1}{\mu}\left(\frac{\partial f}{\partial p_y'}\right)\delta p_y' = \frac{\delta p_y'}{\mu}$$

The Poisson's ratio ν is decided by Eq. (26).

Checking of stress state: The consolidation analysis is carried out by an incremental calculation of each time increment Δt. The decision of unloading in an element is made according to the strain hardening parameter p_y'. Designating the strain hardening parameter at the time $t=t$ and the maximum one before this time by $p_{y,t}'$ and $\bar{p}_y'$ in an element, respectively, in the case of $p_{y,t}' \geqq \bar{p}_y'$, the elasto-plastic matrix $\boldsymbol{D}_{ep}$ is used in the calculation, assuming that the plastic state holds in the element. On the other hand, in the case of $p_{y,t}' < \bar{p}_y'$, the elastic matrix $\boldsymbol{D}_e$ instead of $\boldsymbol{D}_{ep}$ is used, considering that the unloading state is caused in the element.

ANALYTICAL RESULTS AND CONSIDERATIONS

General Remarks

To check the presented finite element formulation, the finite element solution of con-

solidation was compared with the closed form solution by Gibson et al. (1970). The consolidation rate and settlement in both solutions agree well (Matsui et al., 1979). This substantiates the high accuracy of the presented finite element formulation.

To check the applicability of the presented method of elasto-plastic analysis for the K_0-consolidation, the consolidation behavior of a pillar-shaped clay layer, both sides of which are restrained in the horizontal direction, was analyzed (Matsui et al., 1979). As the results, it is confirmed that the presented analytical elasto-plastic model perfectly satisfy requisitions of deformation characteristics of the K_0-consolidation, and that the presented method of consolidation analysis is accurately applicable to the K_0-consolidation analysis, considering the effect of the drainage during incremental loading, and also applicable to such a case that the coefficient of permeability suddenly changes in the layer.

In this chapter, multi-dimensional consolidation analysis is carried out for a partially loaded clay deposit. The detailed descriptions on the analyzed clay layer and surcharge are summarized as follows:

(1) The clay layer is one hundred meter wide and ten meter thick. Its symmetrical half region is descretized by fifty five (5×11) rectangular elements. Numbering of the elements and nodes, referred later on, is shown in Fig. 5.

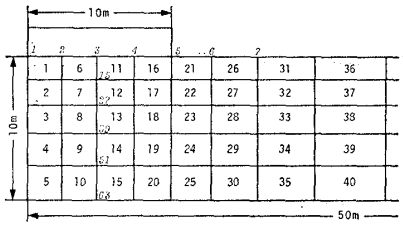

Fig. 5. Numbering of the elements and nodes

(2) A surcharge due to embankment, which is twenty meter wide, is idealized by a strip and flexible load with rough base and is performed up to one meter high with a loading rate of 0.2 m/day. The unit weight of fill material is 1.75 tf/m³ (17.15 kN/m³).

(3) As for the boundary condition of the layer, the bottom is fixed and the sides are without lateral displacement. As for the drainage condition of the layer, both bottom and sides are impervious, while only the top is pervious. The drainage of pore water is permitted even during banking the fill.

(4) The layer is normally K_0-consolidated. The distributions of the initial effective vertical stress σ_{v0}' and the initial void ratio e_0 are shown in Fig. 6 (a) and (b), respectively.

(5) The mechanical characteristics of soft clay of the layer are represented by the presented analytical model

Table 1. Basic mechanical constants of soft clay

λ	κ	M_a	M_p	e_1*	ν	K_0
0.3	0.03	1.485	1.485	2.416	1/3	0.5

* at unit p'

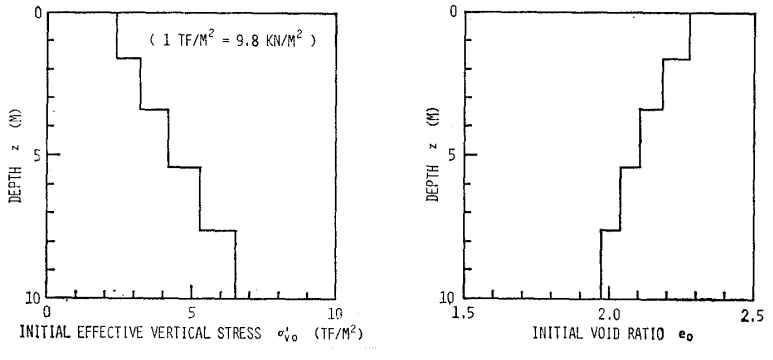

(a) (b)

Fig. 6. Distributions of the initial effective vertical stress σ_{v0}' and the initial void ratio e_0 of clay layer

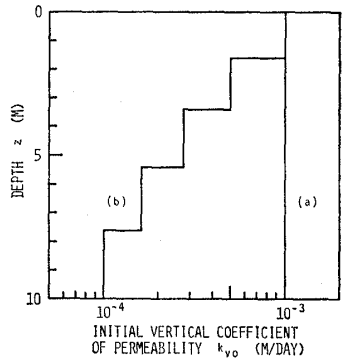

Fig. 7. Distributions of the initial vertical coefficient of permeability k_{v0} of clay layer

previously described, of which the basic mechanical constants are shown in Table 1. The parameters α_a and α_p are approximated by the hyperbola as shown in Fig. 3.

Numerical analyses are carried out for five cases in which various permeabilities are assumed, as shown in Table 2. Fig. 7 shows two types of distributions for the initial vertical coefficient of permeability k_{v0}, each of which is used in the analysis. The horizontal coefficient of permeability k_h is assumed to be equal to or ten times the vertical one k_v, i.e. $k_h/k_v=1$ or 10. The coefficient of permeability during consolidation is constant in case-A, -B, -C and -D, while in case-E varies according to the following equation.

Table 2. Analyzed cases

CASE	CHARACTERISTICS OF PERMEABILITY		
	k_{v0}	k_h/k_v	$k_v(k_h)$DURING CONSOLIDATION
A	a	1	constant
B	a	10	constant
C	b	1	constant
D	b	10	constant
E	a	1	variable*

* according to Eq. (32)

$$k_v=k_{v0}10^{(e-e_0)/0.3} \tag{32}$$

It is not a main purpose of this paper to describe the result of parametric study in detail, which will be presented in subsequent paper. Therefore, the availability of the presented analytical method is demonstrated herein mainly by the result of case-A. Some results of other cases are referred to emphasize the ability and the adequacy of the presented analytical method.

General Nature of Response

Fig. 8 shows the time settlement curves of all cases. The consolidation occurs from the beginning of the loading. The time settlement curves vary unsmoothly at the elapsed time of five days, because of stopping the incremental loading. It is seen in Fig. 8 that the effect of permeability on the consolidation deformation is remarkable. This substantiates that to accurately estimate and introduce into analysis the permeability characteristics of ground, especially its distribution and anisotropy at the initial state and its change involved by the consolidation, is essential to predict the consolidation deformation accurately.

Fig. 9 shows the variations of vertical displacements at the top of the layer with the elapsed time in case-B. It is seen in this figure that the surface of the side area off the surcharge gradually rises even after loading (after five days), and that the rising of node (7) located at a farther position off the surcharge continues for a longer time than at node (6). Such surface rising does not stand out in case-A, which has not the anisotropic permeability.

Fig. 10 shows the variations of horizontal displacements within the layer with the

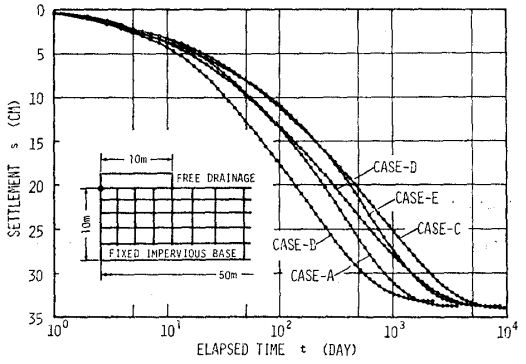

Fig. 8. Time-settlement curves

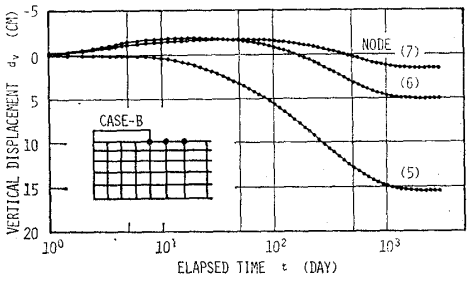

Fig. 9. Variations of vertical displacements at the top of the layer with the elapsed time

elapsed time in case-A. It is seen from this figure that at the upper part of the layer(at node (3), (15) and (27)), a little deformations occur, first, in the lateral direction off the surcharge, followed by lateral deformation in the opposite direction in a certain time. The latter deformations show a time lag with increasing the depth. On the other hand, at the lower part of the layer (at node (39) and (51)), deformations gradually occur only in the lateral direction off the surcharge. To adequately understand the consolidation phenomena, it may be very important to note such deformation behavior within the layer.

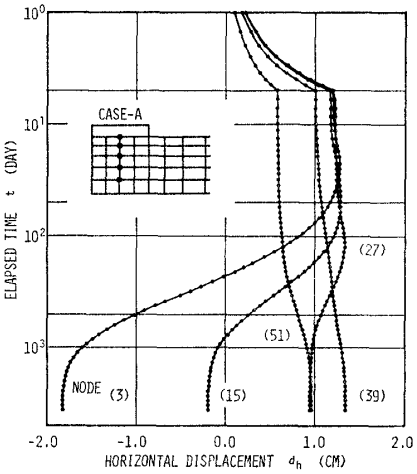

Fig. 10. Variations of horizontal displacements within the layer with the elapsed time

Fig. 11 shows the variations of excess pore water pressure with the elapsed time in case-A. Fig. 11(a) shows the dissipation behavior of the excess pore water pressures of five elements (1) to (5), located at near the center of the surcharge. It is seen from this figure that at the early stage of consolidation the dissipation rate of the excess pore water pressure decreases with inceasing the drainage distance, and that a rise of excess pore water pressure is recognized in the lowest element (element (5)) even after loading (after five days). This phenomena is well known as the Mandel-Cryer effect. Fig. 11 (b) shows the dissipation behavior of five elements (21) to (25), located at near the end of the surcharge. It is seen that the amounts of excess pore water pressures generating in these elements are smaller than in elements (1) to (5), but that their dissipation behaviors are more complicated. This fact may reflect the complexity of stress states in the elements located on the boundary between the active and passive stress states in the layer.

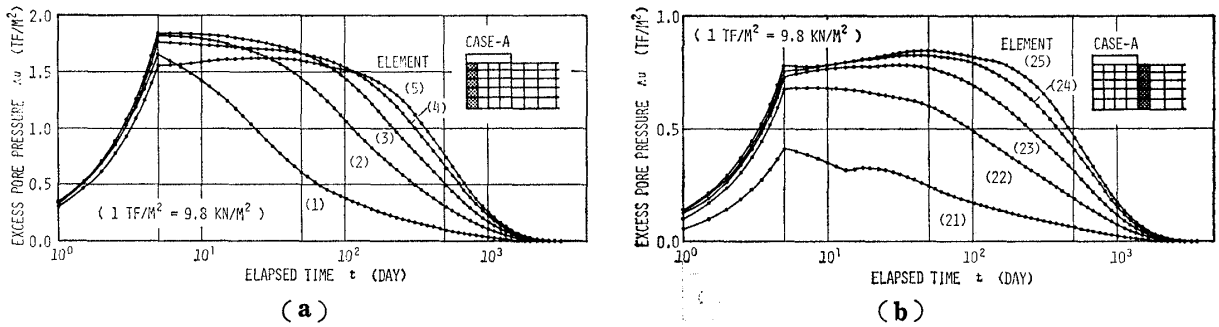

Fig. 11. Variations of excess pore water pressures with the elapsed time

Stress Path Behavior

Transition of the stress state in each element is investigated, considering the relationship with the general nature of response described in the previous section. Fig. 12 shows both effective and total stress paths of representative twelve elements in case-A from the beginning of loading through the end of consolidation. The arrow and the number in Fig. 12 signify the end of loading and the elapsed time in day, respectively, and also TSP and ESP signify the total stress path and the effective stress path, respectively. It can be noticed in Fig. 12 that most of the effective stress paths move on or around the K_0-line. Consequently, as previously emphasized, the important advantage of a model without any singular point on the K_0-line can be again recognized in the consolidation

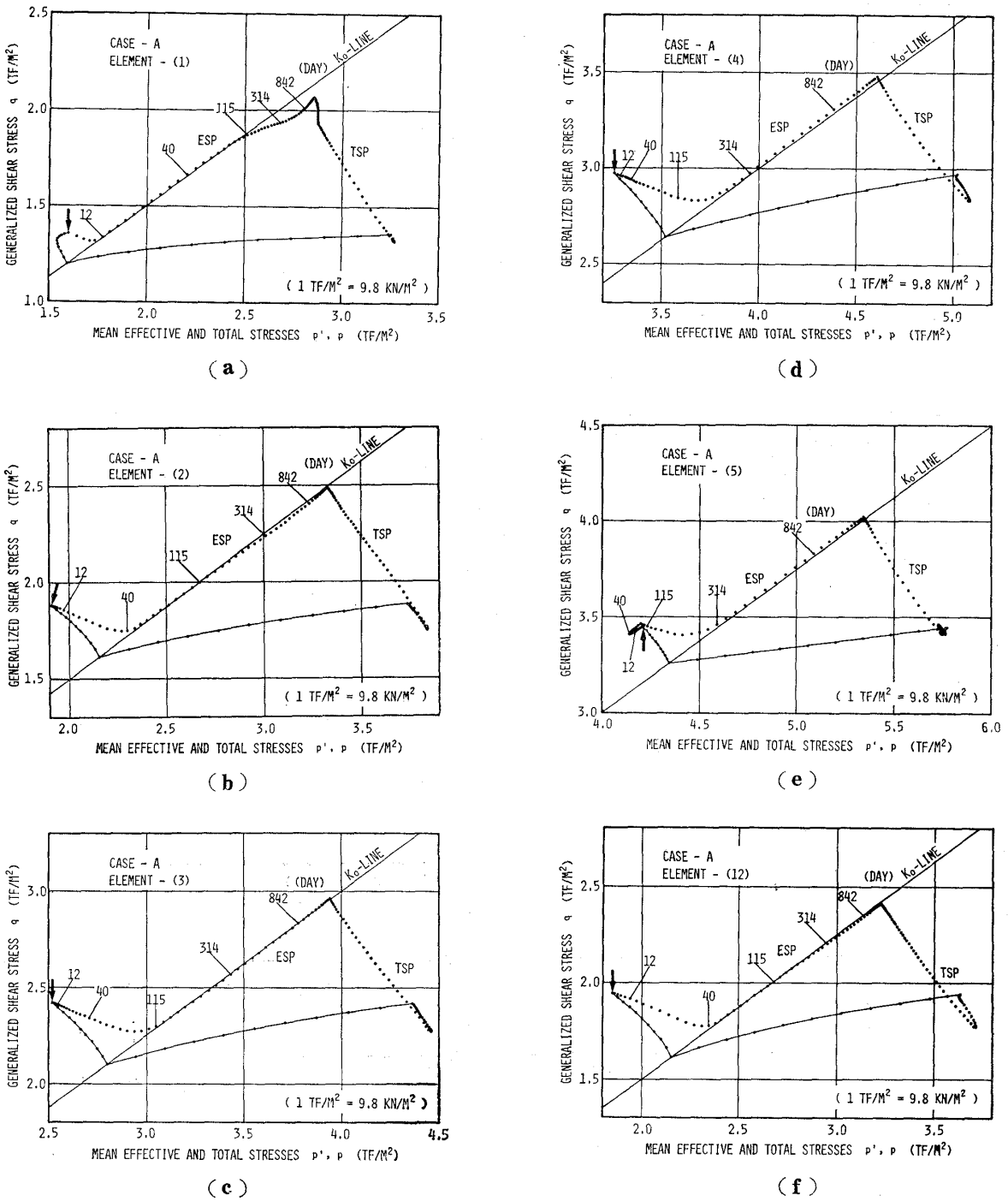

Fig. 12. Effective and total stress paths

analysis of K_0-consolidated layer.

Fig. 12(a) shows the stress paths of element (1) located at the top of the layer near the center of the surcharge. It is recognized in this figure that the effective stress point moves in the direction of increasing the mean effective stress p' even during incremental loading. This is so because in the presented analytical method the drainage is permitted even during incremental loading. In about twelve days after loading, the effective stress point reaches the K_0-line, and since then moves up along the K_0-line. In more than one hundred days after loading, it crosses the K_0-line and comes into the

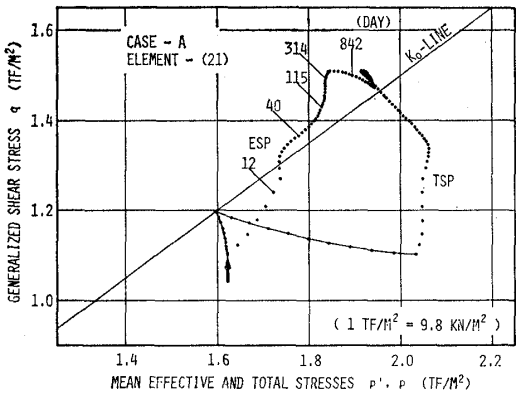

(g)

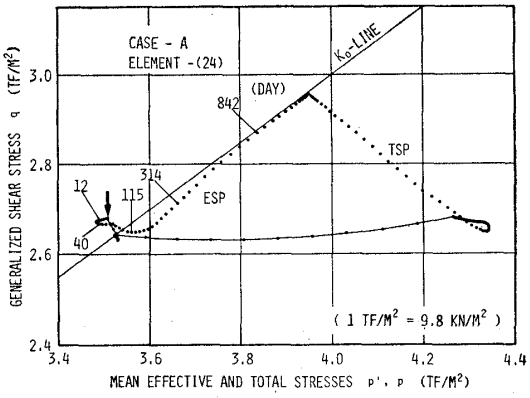

(j)

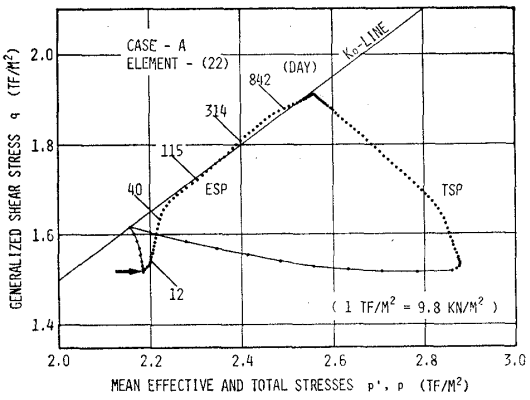

(h)

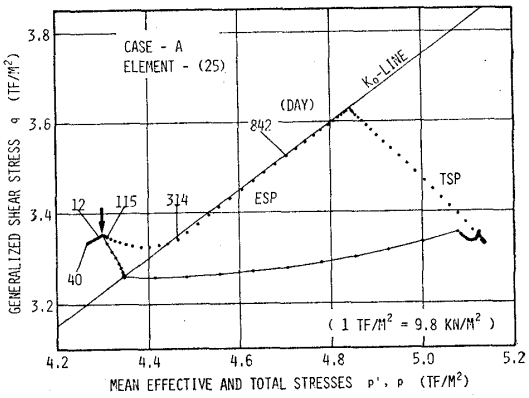

(k)

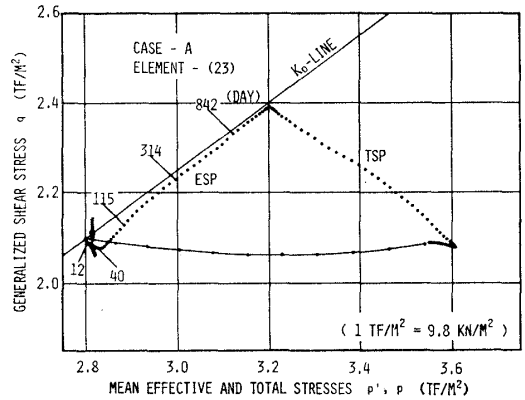

(i)

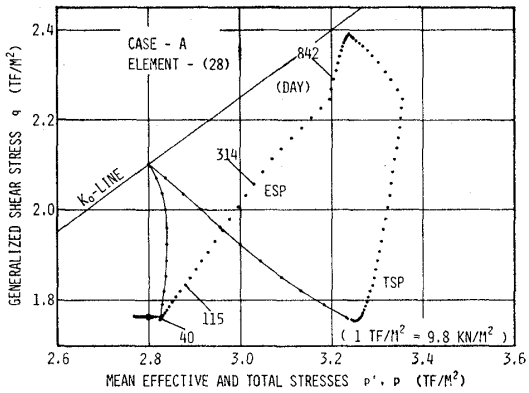

(l)

during multi-dimensional consolidation

passive stress state, and then meets total stress point. The consolidation is completed there. This shift of the effective stress point from the active stress state to the passive is a response corresponding to the reversal of the lateral deformation in the upper part of the layer, as shown in Fig. 10.

Figs. 12 (b), (c), (d) and (e) show the stress paths of elements (2), (3), (4) and (5), respectively, which are located below element (1) in order of increasing depth. Comparing these stress paths behaviors, their differences in the time-dependent consolidation behavior and the stress state-dependent behavior reflect well the characteristics of the

positions of each element.

The stress path of element (5) shows a specially interesting behavior. As shown in Fig. 12(e), just after the end of loading the effective stress point moves in the direction of decreasing the mean effective stress p', occurring the unloading within the element, while the total stress point little moves in the direction of the mean total stress p. Consequently, the excess pore water pressure increases. Such behavior in element (5) corresponds to that in Fig. 11(a), in which the Mandel-Cryer effect generates. In due time, the effective stress point reverses in the direction of increasing p' and comes into the elasto-plastic state. Similar behaviors can be found on the stress path behaviors of elements (23), (24) and (25) shown in Figs. 12 (i), (j) and (k), respectively, in which the Mandel-Cryer effect also generates.

Fig. 12(g) shows the stress paths of element (21) located at the top of the layer near the end of the surcharge. As shown in Fig. 11(b), the excess pore water pressure of element (21) does not gradually decrease, but temporarily increases. Judging from the stress path behavior, this phenomena may come from the rapid shift of effective stress point from the passive stress state to the active.

Figs. 12(i) and (j) show the stress paths of elements (23) and (24), located on the boundary between the active and passive stress regions in the layer. The initial movement of their effective stress paths is complicated, because the reversal of shear direction and the unloading behavior are involved in.

Fig. 12(f) shows the stress paths of element (12), in which the largest stress ratio generates at the end of loading. Fig. 12 (l) shows the stress paths of element (28), which is an example of elements in the passive stress state.

As shown above, the process of multi-dimensional elasto-plastic consolidation is very complicated, because the rate of excess pore pressure generation depends on the shear deformation during consolidation involving the dilatancy effect of clay.

Increasing Trend of the Undrained Strength due to Consolidation

In stage construction method, which is often introduced into banking construction on soft clay deposit, it is important to understand the increasing trend of the undrained strength due to consolidation. The presented method of elasto-plastic consolidation analysis can give informations on it. This is one of important advantages of the presented method, in which a strain hardening model is used.

Fig. 13 shows the variation of the strain hardening parameter p_y' of the marked six elements with the elapsed time in case-A. The ordinate of Fig. 13 is represented by the degree of strain hardening based on the strain hardening parameters at both ends of loading (five days) and consolidation. It is possible to estimate the variation of the potential undrained strength of clay during consolidation by means of that of the strain hardening parameter. In Fig. 13, the degree of settlement U is also shown.

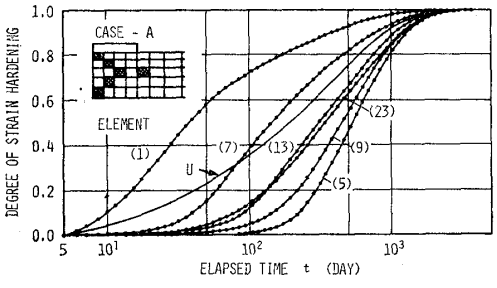

Fig. 13. Variations of the strain hardening parameter p_y' with the elapsed time

It is seen from Fig. 13 that the deeper the element is located on, the more the strain hardening is delayed. Because the strain hardening is caused by the plastic volumetric strain, it should reflect the drainage behavior within layer.

The degree of strain hardening is generally delayed more than that of settlement.

Especially, it is noted that even in element (7) located at near the top surface such a delay is caused at the early stage of consolidation. Thus, it is not considered that the conventional degree of settlement can represent the increasing trend of the undrained strength in the whole layer. Elements (13) and (23), both of which are located at a same depth, have a little bit different strain hardening trends. This difference may be suggestive.

CONCLUSION

In this paper have been presented a sophisticated technique of multi-dimensional elasto-plastic consolidation analysis due to finite element method. The main conclusions obtained are summarised as follows:

(1) The finite element formulation for consolidation is presented, which gives a solution of the sufficient accuracy comparing with the closed form solution.

(2) An elasto-plastic analytical model of clay is proposed, which is reasonably applicable to the elasto-plastic analysis of the K_0-consolidation.

(3) The presented method of consolidation analysis is also characterized by the ability to analyze such cases that the drainage is permitted even during incremental loading and that the permeability suddenly changes in the layer. It is clarified that these abilities of the presented technique make a more realistic consolidation analysis possible.

(4) Multi-dimensional consolidation analysis is carried out for partially loaded ground model in the K_0-state, using the proposed elasto-plastic model. The resulting deformation and stress path behaviors substantiate the validity of the presented technique, which brings out some behaviors reflecting the real mechanism of consolidation of clay.

Thus, the presented method of consolidation analysis may provide a useful technique for the practical consolidation analysis of clay deposit, and the results may offer important clues to solve the complicated consolidation behaviors.

ACKNOWLEDGEMENTS

The authors are indebted to Professor T. Ito, at the Osaka University, for his kind support and encouragement. They wish also to express their gratitude to Messrs. T. Yamamoto and A. Tamura for their assistance of numerical calculations. This work was performed with the financial support of Grant-in-Aid for Scientific Research, the Ministry of Education. This support is gratefully acknowledged.

NOTATION

A=hardening coefficient

$\boldsymbol{a}=\left\{\frac{\partial f}{\partial \sigma_x'} \frac{\partial f}{\partial \sigma_y'} \frac{\partial f}{\partial \tau_{xy}}\right\}^T$

$\boldsymbol{B}$=matrix defined by Eq. (8)

$\boldsymbol{b}_4, \boldsymbol{b}_5$=vectors of the fourth and fifth rows of $\boldsymbol{B}^{-1}$, respectively

$\boldsymbol{C}$=vector transforming the representative excess pore water pressure increment into the volume change of element

$\boldsymbol{D}_e$=nonlinear elastic stress-strain matrix

$\boldsymbol{D}_{ep}$=elasto-plastic stress-strain matrix

E=nonlinear elastic modulus

e=void ratio

$\Delta \boldsymbol{F}$=incremental vector of the equivalent nodal force

f_a, f_p=yield functions for the active and passive stress states, respectively

$\boldsymbol{K}$=stiffness matrix of element

K_0=coefficient of earth pressure at rest
k_x, k_y=coefficients of permeability in the directions of x and y, respectively
k_v, k_h=coefficients of permeability in the vertical and horizontal directions, respectively
$\boldsymbol{L}$=vector transforming the nodal displacement increment into the volume change of element
p'=mean effective principal stress
p_y'=strain hardening parameter
$\bar{p}_y'$=maximum p_y' of element before time $t=t$
q=generalized shear stress
t=real time
$\Delta \boldsymbol{U}$=incremental vector of the nodal displacement
u=excess pore water pressure
$\bar{u}$=representative excess pore water pressure
V=volume of element
ΔV=volume change of element
v=volumetric strain
$\bar{x}, \bar{y}$=local co-ordinate of the center of element
$\alpha_1, \alpha_2, \alpha_3, \alpha_4, \alpha_5$=coefficients on the distribution of representative excess pore water pressure
α_a, α_p=parameters on the plastic strain increment ratio for the active and passive stress states, respectively
γ=generalized shear strain
γ_w=unit weight of pore water
γ_{xy}=shear strain
$\varepsilon_1, \varepsilon_2, \varepsilon_3$=principal strains
$\varepsilon_x, \varepsilon_y$=normal strains in the directions of x and y, respectively
ε_v=vertical strain
η=stress ratio ($=q/p'$)
$\eta_{ko}=\eta$ on the K_0-line
θ=constant on the difference approximation
κ=swelling index
λ=compression index
$M_a, M_p=\eta$ at the critical state in the active and passive stress states, respectively
μ=non-negative scalar quantity
ν=Poisson's ratio
$\sigma_1', \sigma_2', \sigma_3'$=effective principal stresses
σ_v'=effective vertical stress
σ_x', σ_y'=effective normal stresses in the directions of x and y, respectively
τ_{xy}=shear stress
$1/\psi$=plastic strain increment ratio ($=\delta\gamma^p/\delta v^p$)

REFERENCES

1) Akai, K. and Tamura, T. (1977): "Numerical analysis of stress path under multi-dimensional consolidation," Proc., Specialty Session 12, 9 th ICSMFE, Tokyo, pp. 30-53.
2) Biot, M. A. (1941): "General theory of three-dimensional consolidation," J. Appl. Phys., Vol. 12, pp. 155-164.
3) Christian, J. T. (1968): "Undrained stress distribution by finite elements," J. Soil Mech. Found. Div., ASCE, Vol. 94, No. SM 6, pp. 1333-1345.
4) Christian, J. T. and Boehmer, J. W. (1970): "Plane strain consolidation by finite elements," J. Soil Mech. Found. Div., ASCE, Vol. 96, No. SM 4, pp. 1435-1457.
5) Christian, J. T., Boehmer, J. W. and Martin, P. P. (1972): "Consolidation of a layer under a strip load," J. Soil Mech. Found. Div., ASCE, Vol. 98, No. SM 7, pp. 693-707.
6) Desai, C. S. and Saxena, S. K. (1977): "Consolidation analysis of layered anisotropic foundations," Int. J. Numer. and Analy. Methods Geomech., Vol. 1, pp. 5-13.

7) Gibson, R. E., Schiffman, R. L. and Pu, S. L. (1970): "Plane strain and axially symmetric consolidation of a clay layer on a smooth impervious base," Q. J. Mech. and Applied Math., Vol. 23, pp. 505-520.
8) Ghaboussi, J. and Wilson, E. L. (1973): "Flow of compressible fluid in porous elastic media," Int. J. Numer. Methods Eng., Vol. 5, No. 3, pp. 419-442.
9) Herrmann, L. R. (1965): "Elasticity equations for incompressible and nearly incompressible materials by a variational theorem," AIAA J., Vol. 3, pp. 1896-1900.
10) Hwang, C. T., Morgenstern, N. R. and Murry, D. W. (1971): "On solutions of plane strain consolidation problems by finite element methods," Can. Geotech. J., Vol. 8, pp. 109-118.
11) Hwang, C. T., Morgenstern, N. R. and Murry, D. W. (1972): "Application of the finite element method to consolidation problems," Proc., Symp. Applications of finite element method in geomechanical engineering, Vicksburg, USA, pp. 739-765.
12) Matsui, T., Abe, N. and Tamura, A. (1979): "Multi-dimensional consolidation analysis of saturated clay," Proc., 14 th Japan National Conference on SMFE, pp. 237-240 (in Japanese).
13) Ohta, H. and Hata, S. (1971): "On the state surface of anisotropically consolidated clays," Proc., JSCE, No. 196, pp. 117-124.
14) Roscoe, K. H., Schofield, A. N. and Thurairajah, A. (1963): "Yielding of calys in states wetter than critical," Geotechnique, Vol. 13, No. 2, pp. 211-240.
15) Roscoe, K. H. and Burland, J. B. (1968): "On the generalized stress-strain behaviour of wet clay," Engineering Plasticity, Cambridge University Press, pp. 535-609.
16) Sandhu, R. S. and Wilson, E. L. (1969): "Finite element analysis of seepage in elastic media," J. Eng. Mech. Div., ASCE, Vol. 95, No. EM 3, pp. 641-652.
17) Smith, I. M. and Hobbs, R. (1976): "Biot analysis of consolidation beneath embankments," Geotechnique, Vol. 26, No. 1, pp. 149-171.
18) Valliappan, S. and Lee, I. K. (1975): "Consolidation of nonhomogeneous anisotropic layered soil media," Proc., 2 nd Australia-Newzealand conference on geomechanics, Brisbane, pp. 67-71.
19) Wilson, C. P. (1965): "Structural analysis of axisymmetric solids," AIAA J., Vol. 3, pp. 2269-2274.
20) Wroth, C. P. and Zytynski, M. (1977): "Finite element computations using an elasto-plastic soil model for geotechnical problems of soft clay," Proc., Specialty Session 12, 9 th ICSMFE, Tokyo, pp. 193-243.
21) Yokoo, Y., Yamagata, K. and Nagaoka, H. (1971a): "Finite element method applied to Biot's consolidation theory," Soils and Foundations, Vol. 11, No. 1, pp. 29-46.
22) Yokoo, Y., Yamagata, K. and Nagaoka, H. (1971b): "Finite element analysis of consolidation following undrained deformation", Soils and Foundations, Vol. 11, No. 4, pp. 37-58.

(Received April 2, 1980)